REPORT DOCUMENTATION PAGE

Form Approved OMB NO. 0704-0188

1. REPORT DATE (DD-MM-YYYY)	2. REPORT TYPE	3. DATES COVERED (From - To)
	Technical Report	-

4. TITLE AND SUBTITLE
Analytical Solution for Flexural Response of Epoxy Resin Materials

5a. CONTRACT NUMBER
W911NF-07-1-0132

5b. GRANT NUMBER

5c. PROGRAM ELEMENT NUMBER
611102

6. AUTHORS
Masoud Yekani Fard, Yingtao Liu, Aditi Chattopadhyay

5d. PROJECT NUMBER

5e. TASK NUMBER

5f. WORK UNIT NUMBER

7. PERFORMING ORGANIZATION NAMES AND ADDRESSES
Arizona State University
Office of Research & Sponsored Projects Administration
Arizona State University
Tempe, AZ 85287 -3503

8. PERFORMING ORGANIZATION REPORT NUMBER

9. SPONSORING/MONITORING AGENCY NAME(S) AND ADDRESS(ES)
U.S. Army Research Office
P.O. Box 12211
Research Triangle Park, NC 27709-2211

10. SPONSOR/MONITOR'S ACRONYM(S)
ARO

11. SPONSOR/MONITOR'S REPORT NUMBER(S)
49008-EG.5

12. DISTRIBUTION AVAILIBILITY STATEMENT
Approved for Public Release; Distribution Unlimited

13. SUPPLEMENTARY NOTES
The views, opinions and/or findings contained in this report are those of the author(s) and should not contrued as an official Department of the Army position, policy or decision, unless so designated by other documentation.

14. ABSTRACT
A multilinear parametric uniaxial stress strain approach has been used to obtain the closed form nonlinear moment curvature response based on strain compatibility in bending for epoxy resin materials. The stress strain curves, consisting of a bilinear ascending curve followed by strain softening and constant plastic flow in tension and compression, are described by two main parameters in addition to five non-dimensional tensile and seven non-dimensional compressive parameters. The main parameters are modulus of elasticity and strain at the

15. SUBJECT TERMS
polymer, stress strain relations, moment distribution, curvature, load, deflection, localization, nonlinear response

16. SECURITY CLASSIFICATION OF:			17. LIMITATION OF ABSTRACT	15. NUMBER OF PAGES	19a. NAME OF RESPONSIBLE PERSON
a. REPORT	b. ABSTRACT	c. THIS PAGE			Aditi Chattopadhyay
UU	UU	UU	UU		19b. TELEPHONE NUMBER 480-965-9342

Report Title

Analytical Solution for Flexural Response of Epoxy Resin Materials

ABSTRACT

A multilinear parametric uniaxial stress strain approach has been used to obtain the closed form nonlinear moment curvature response based on strain compatibility in bending for epoxy resin materials. The stress strain curves, consisting of a bilinear ascending curve followed by strain softening and constant plastic flow in tension and compression, are described by two main parameters in addition to five non-dimensional tensile and seven non-dimensional compressive parameters. The main parameters are modulus of elasticity and strain at the proportional elastic limit point in tension. Parametric studies show that ultimate tensile stress and compressive yield stress as well as tension and compression flow stresses have the highest effects on flexural load carrying capacity. Moment curvature equations in conjunction with deformation localization and static equilibrium conditions were used to simulate the flexural load deflection response of a beam under three-point bending condition. The simulations reveal that the direct use of uniaxial tensile and compressive stress strain curves underestimates the flexural response due to the differences in the effective volume of the material subjected to critical stresses.

Analytical Solution for Flexural Response of Epoxy Resin Materials

Masoud Yekani Fard[1], Yingtao Liu[2], and Aditi Chattopadhyay[3]

Abstract

A multilinear parametric uniaxial stress strain approach has been used to obtain the closed form nonlinear moment curvature response based on strain compatibility in bending for epoxy resin materials. The stress strain curves, consisting of a bilinear ascending curve followed by strain softening and constant plastic flow in tension and compression, are described by two main parameters in addition to five non-dimensional tensile and seven non-dimensional compressive parameters. The main parameters are modulus of elasticity and strain at the proportional elastic limit point in tension. Parametric studies show that ultimate tensile stress and compressive yield stress as well as tension and compression flow stresses have the highest effects on flexural load carrying capacity. Moment curvature equations in conjunction with deformation localization and static equilibrium conditions were used to simulate the flexural load deflection response of a beam under three-point bending condition. The simulations reveal that the direct use of uniaxial tensile and compressive stress strain curves underestimates the flexural response due to the differences in the effective volume of the material subjected to critical stresses.

[1]Graduate Student, Department of Mechanical and Aerospace Engineering, Arizona State University, masoud.yekanifard@asu.edu

[2] Graduate Student, Department of Mechanical and Aerospace Engineering, Arizona State University

[3] Professor, Department of Mechanical and Aerospace Engineering, Arizona State University

CE Database subject headings: polymer, stress strain relations, moment distribution, curvature, load, deflection, localization, nonlinear response

Introduction

Stress strain curves of polymeric materials are still a challenge for researchers. Difficulty of a constitutive law in polymeric material is mainly due to the characterization of its mechanical behavior under different kind of loading conditions. The hydrostatic component of stress has a significant effect on the load deformation response of resins even at low levels of stress (Ward and Sweeny 2004). Hydrostatic stresses are known to affect the yield stress and nonlinear response of epoxy resin materials. In order to develop a general model for polymeric materials, their behavior under different types of loading conditions has to be understood.

Several constitutive models have been proposed for polymeric materials in the past three decades. The most successful models are proposed by groups at Oxford (Buckley and Jones 1995; Buckley and Dooling 2004), MIT (Boyce et al. 1989; Boyce et al. 1994; Hasan and Boyce 1995; Mulliken and Boyce 2006), and Eindhoven (Tervoort et al. 1996; Tervoort et al. 1998; Govaert et al., 2000). These models have been successful, especially, in fitting quasi-static inplane test results. Wineman and Rajagopal (2000) used a viscoplasticity model to capture the behavior of polymers. Zhang and Moore (1997), and Gilat et al. (2007) modified the Bodner–Partom model originally developed for metals to obtain the nonlinear uniaxial response of polymeric materials. By modifying the definitions of the effective stress and effective inelastic strain rate in the Drucker-Prager yield criteria, Li and Pan (1990), Chang and Pan (1997), and Hsu et al. (1999) developed an approach for the constitutive law of polymeric materials. Jordan et al. (2008) modified

the original model of Mulliken and Boyce (2006) for one dimension to capture the compressive mechanical properties of polymer composites. The original model is a three dimensional model for thermoplastic polymers. Lu et al. (2001) used the constitutive model developed by Hasan and Boyce (1995) to simulate the experimental results on the uniaxial compressive stress strain behavior of epon E 828/T-403. Chen et al. (1998) modeled the uniaxial compressive response of epon E 828/T-403 using Johnson-Cook model (Johnson 1983). They simulated the experimental compression response up to 10% of true strain, but reported experimental stress strain curves showing elastic deformation, a yield-like peak, and a strain softening region up to around 35%. The majority of the parameters were determined by fitting the model to experimental tensile and compressive data. Naaman and Reinhardt (2006) used multi linear stress strain and stress crack opening approaches to characterize the mechanical behavior of high performance fiber reinforced cement composites. Hobbiebrunken et al. (2007) and Goodier (1993) studied the correlation between presence of defects (voids and micro cracks) and the volume under stress in epoxy resin glassy polymers. The crack initiation by void nucleation or a pre-existing flaw in epoxy resins was observed and the dependency of the failure behavior and strength on the size effect, stress state, and the volume of the body subjected to stress was studied (Hobbiebrunken et al. 2007, Bazant and Chen 1997; Odom and Adam 1992). Flexural strength distributions and ratio of flexural strength to tension strength of epoxy resin and PMMA materials were studied using Weibull model (Giannotti et al. 2003; Vallo 2002). Giannotti et al. (2003) used a modified two-parameter Weibull model to compare the effect of loading systems on the mean stress in polymeric

materials, and observed that it predicts a mean flexural strength up to 40% higher than the mean tensile strength for Weibull modulus greater than 14.

This study is motivated by the need to better characterize the flexural behavior of epoxy resin materials. Closed form solutions for moment curvature response were derived based on nonlinear tension and compression stress strain curves. The results were expressed in normalized form to eliminate the effects of sizes and strength of specimen. A technique based on the uniaxial tension and compression stress strain relations, strain compatibility in bending, static equilibrium, deformation localization, and moment area method was used to simulate flexural load deflection response in a statically determinate structure. Since the solution is derived explicitly, iterative procedures required for handling material nonlinearity are not required; hence this method is powerful for forward and inverse analyses. The effects of different segments of tension and compression stress strain curves for improving the flexural performance of epoxy resin materials were studied. The purpose of this study is two folds: (i) to correlate the uniaxial tension and compression material response with flexural behavior in epoxy resins; (ii) to evaluate the effect of different segments of tension and compression stress strain curve on flexural response.

Strain Softening With Plastic Flow in Tension and Compression

Epoxy resin materials share some similarities such that while the compressive and tensile moduli are approximately equal, the first point showing deviation from linearity in the stress strain curve in tension is weaker than the one in compression stress strain curve (Ward and Sweeney 2004). It is critically important to observe that the general shapes of the stress strain curves in tension and compression in epoxy resin materials are similar as

they represent initial linear behavior followed by an ascending curve with reduced stiffness in the pre-peak region, and strain softening response in the post-peak region (G'Sell and Souahi 1997; Boyce and Arruda 1990; Buckley and Harding 2001; Shah khan et al. 2001; Jordan et al. 2008; Littell et al. 2008; Chen et al. 2001). Fig. 1 shows the complete tension and compression stress strain curves. The two parameters characterizing the tensile response in the pre-peak region are Proportionality Elastic Limit (PEL) and Ultimate Tensile Strength (UTS). Post-peak region in tension model is expressed with slope of softening ($E_{soft,t}$), plastic flow (σ_f), and the ultimate strain (ε_{Ut}). Yield stress is often assumed to be equal to the first peak stress in the stress strain curve. Pre-peak region in compression is characterized by Proportionality Elastic Limit in compression (PEL,c) and Compressive Yield Stress (CYS). The post-peak response in compression is determined by slope of softening ($E_{soft,c}$), compression plastic flow ($\sigma_{f,c}$), and the compressive ultimate strain (ε_{Uc}). The tension and compression strain stress model is defined in Table 1.

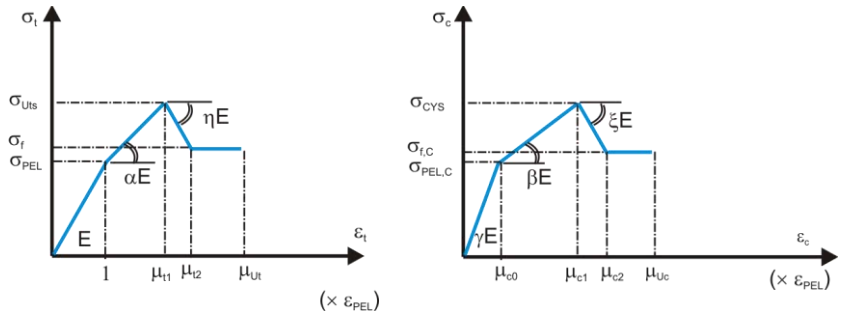

Fig. 1 Bilinear ascending curve and strain softening post peak response in tension and compression

Table 1: Definition of stress in tension and compression

Stress	Definition	Domain of strain
$\sigma_t(\varepsilon_t)$	$E\varepsilon_t$	$0 \le \varepsilon_t \le \varepsilon_{PEL}$

	$E\,(\varepsilon_{PEL} + \alpha\,(\varepsilon_t - \varepsilon_{PEL}))$	$\varepsilon_{PEL} < \varepsilon_t \le \mu_{t1}\,\varepsilon_{PEL}$
	$E\,(\varepsilon_{PEL} + \alpha\,\varepsilon_{PEL}\,(\mu_{t1}-1) + \eta\,(\varepsilon_t - \mu_{t1}\varepsilon_{PEL}))$	$\mu_{t1}\,\varepsilon_{PEL} < \varepsilon_t \le \mu_{t2}\,\varepsilon_{PEL}$
	$E\,(\varepsilon_{PEL} + \alpha\,\varepsilon_{PEL}\,(\mu_{t1}-1) + \eta\varepsilon_{PEL}\,(\mu_{t2} - \mu_{t1}))$	$\mu_{t2}\,\varepsilon_{PEL} < \varepsilon_t \le \mu_{Ut}\,\varepsilon_{PEL}$
	0	$\mu_{Ut}\,\varepsilon_{PEL} < \varepsilon_t$
	$\gamma E\,\varepsilon_c$	$0 \le \varepsilon_c \le \mu_{c0}\,\varepsilon_{PEL}$
	$E(\gamma\,\mu_{c0}\,\varepsilon_{PEL} + \beta\,(\,\varepsilon_c - \mu_{c0}\,\varepsilon_{PEL}))$	$\mu_{c0}\,\varepsilon_{PEL} < \varepsilon_c \le \mu_{c1}\,\varepsilon_{PEL}$
$\sigma_c(\varepsilon_c)$	$E(\gamma\,\mu_{c0}\,\varepsilon_{PEL} + \beta\;\varepsilon_{PEL}\,(\mu_{c1} - \mu_{c0}) + \xi(\varepsilon_c - \mu_{c1}\varepsilon_{PEL}))$	$\mu_{c1}\,\varepsilon_{PEL} < \varepsilon_c \le \mu_{c2}\,\varepsilon_{PEL}$
	$E(\gamma\,\mu_{c0}\,\varepsilon_{PEL} + \beta\;\varepsilon_{PEL}\,(\mu_{c1} - \mu_{c0}) + \xi\,\varepsilon_{PEL}\,(\mu_{c2} - \mu_{c1}))$	$\mu_{c2}\,\varepsilon_{PEL} < \varepsilon_c \le \mu_{Uc}\,\varepsilon_{PEL}$
	0	$\mu_{Uc}\,\varepsilon_{PEL} < \varepsilon_c$

The complete tension and compression stress strain curves are defined uniquely by two material parameters: modulus of elasticity in tension (E), and strain at the tensile proportionality elastic limit (ε_{PEL}), and twelve normalized parameters: μ_{t1}, μ_{t2}, μ_{Ut}, μ_{co}, μ_{c1}, μ_{c2}, μ_{Uc}, α, η, γ, β, and ξ. The tensile and compressive stresses at the PEL point are related empirically to the stresses at the UTS and CYS points. Elastic modulus in tension and compression are practically identical (Foreman et al. 2010). However, bi-modulus material constants ($\gamma \neq 1$) are considered in tension and compression. Equations (1) to (3) show the definitions of the normalized parameters.

$$\mu_{c0} = \frac{\varepsilon_{PEL,c}}{\varepsilon_{PEL}},\ \mu_{c1} = \frac{\varepsilon_{CYS}}{\varepsilon_{PEL}},\ \mu_{c2} = \frac{\varepsilon_{Sc}}{\varepsilon_{PEL}},\ \mu_{t1} = \frac{\varepsilon_{Uts}}{\varepsilon_{PEL}},\ \mu_{t2} = \frac{\varepsilon_{St}}{\varepsilon_{PEL}} \tag{1}$$

$$\mu_{Uc} = \frac{\varepsilon_{Uc}}{\varepsilon_{PEL}}, \mu_{Ut} = \frac{\varepsilon_{Ut}}{\varepsilon_{PEL}} \tag{2}$$

$$\gamma = \frac{E_c}{E}, \beta = \frac{E_{PEL,c}}{E},\quad \xi = \frac{E_{soft,c}}{E},\ \alpha = \frac{E_{PEL,t}}{E},\ \eta = \frac{E_{soft,t}}{E} \tag{3}$$

Closed-form Moment Curvature Response

Strain compatibility in bending is considered to derive moment curvature relationship for a rectangular cross section with the width of *b* and the depth of *h*. Using the stress strain relationships in Fig. 1 and the known applied compressive strain at the top fiber ($\lambda\varepsilon_{PEL}$), sixteen different cases of strain and stress distributions are shown in Fig. 2. The development of the stress strain relation across the cross section, and the possibilities of tension or compression failures are presented in Table 2. In this approach, moving through different stages depends on the transition points (tp_{ij}) which are functions of material parameters. Indices *i* and *j* refer to origin and destination stages, respectively. Stress strain develops at least to stage 4 where compressive and tensile failure is possible if $\lambda_{max} = \mu_{Uc}$ in case 10, or $\lambda_{max} = J$ in case 9. Characteristic points, *A* to *P*, are calculated as functions of material parameters to satisfy the following relation at each load step.

$$\varepsilon_t \leq \Omega\,\varepsilon_{PEL} \tag{4}$$

Where ε_t is the tensile strain at the bottom fiber and Ω, depending on the case of stress distribution, is one of the followings: 1, μ_{t1}, μ_{t2}, μ_{Ut}. ε_t is expressed as a linear function of the applied compressive strain at the top fiber (ε_c)

$$\varepsilon_t = \frac{1-\kappa}{\kappa}\varepsilon_c \tag{5}$$

Where ε_c is equal to $\lambda\,\varepsilon_{PEL}$ and κ is the depth of the neutral axis which is a function of material parameters. Characteristic points *A* and *B* are presented in Equation (6) as an example. As the applied strain parameter λ is incrementally imposed, the strain and stress distribution is determined and the internal tension and compression forces are computed. For instance, the internal forces for the tension and compression subzones for case

sixteen (Fig. 2-q) normalized to the tension force at the PEL point ($bhE\varepsilon_{PEL}$) are as shown in Equations (7) to (14).

$$A=\frac{\sqrt{\gamma}-1}{\gamma-\sqrt{\gamma}},\ B=\frac{\mu_{c0}(\beta-\gamma)+\sqrt{\mu_{c0}^2\gamma(\gamma-\beta)+\beta}}{\beta} \tag{6}$$

$$\frac{F_{t1}}{bhE\varepsilon_{PEL}}=\frac{\kappa}{2\lambda} \tag{7}$$

$$\frac{F_{t2}}{bhE\varepsilon_{PEL}}=\frac{(2+\alpha\mu_{t1}-\alpha)(\mu_{t1}-1)\kappa}{2\lambda} \tag{8}$$

$$\frac{F_{t3}}{bhE\varepsilon_{PEL}}=\frac{(2+2\alpha(\mu_{t1}-1)+\eta(\mu_{t2}-\mu_{t1}))(\mu_{t2}-\mu_{t1})\kappa}{2\lambda} \tag{9}$$

$$\frac{F_{t4}}{bhE\varepsilon_{PEL}}=\frac{(1+\alpha(\mu_{t1}-1)+\eta(\mu_{t2}-\mu_{t1}))(-\lambda-\mu_{t2})\kappa}{\lambda}+1+\alpha(\mu_{t1}-1)+\eta(\mu_{t2}-\mu_{t1}) \tag{10}$$

$$\frac{F_{c1}}{bhE\varepsilon_{PEL}}=\frac{\gamma\mu_{c0}^2\kappa}{2\lambda} \tag{11}$$

$$\frac{F_{c2}}{bhE\varepsilon_{PEL}}=\frac{(\mu_{c1}-\mu_{c0})(2\gamma\mu_{c0}+\beta(\mu_{c1}-\mu_{c0}))\kappa}{2\lambda} \tag{12}$$

$$\frac{F_{c3}}{bhE\varepsilon_{PEL}}=\frac{(\mu_{c2}-\mu_{c1})(2\gamma\mu_{c0}+2\beta(\mu_{c1}-\mu_{c0})+\xi(\mu_{c2}-\mu_{c1}))\kappa}{2\lambda} \tag{13}$$

$$\frac{F_{c4}}{bhE\varepsilon_{PEL}}=\frac{(\lambda-\mu_{c2})(\gamma\mu_{c0}+\beta(\mu_{c1}-\mu_{c0})+\xi(\mu_{c2}-\mu_{c1}))\kappa}{\lambda} \tag{14}$$

Net force is calculated as the difference between the tension and compression forces for each case. By applying internal equilibrium, the value of κ is obtained. The expressions of net force in some stages result in more than one solution for κ. For an isotropic material, the first κ value is 0.5 since the neutral axis coincides with the centroid of the rectangular section. Since the neutral axis changes incrementally, the next value of

κ is the closest to the previous neutral axis. Using a large amount of numerical tests covering possible ranges of material parameters, the solution of κ which yields a valid value $0 < \kappa < 1$, is determined. For instance, the κ for case sixteen (Fig. 2-q) is as below

$$\kappa_{16} = \left(\begin{array}{c} \dfrac{(\lambda-\mu_{c0})^2(\gamma-\beta)+(\lambda-\mu_{c1})^2(\beta-\xi)+\xi(\lambda-\mu_{c2})^2+(\lambda+\mu_{t1})^2(\eta-\alpha)}{-2\lambda(1+\alpha(\mu_{t1}-1)+\eta(\mu_{t2}-\mu_{t1}))} + \\ \dfrac{-\eta(\lambda+\mu_{t2})^2+\alpha(\lambda+1)^2-\gamma\lambda^2-2\lambda-1}{-2\lambda(1+\alpha(\mu_{t1}-1)+\eta(\mu_{t2}-\mu_{t1}))} \end{array} \right)^{-1} \quad (15)$$

Moment expressions are obtained by taking the first moment of the compression and tension forces about the neutral axis. Curvature is calculated by dividing the top compressive strain by the depth of the neutral axis κh. The general equations for normalized moment and curvature are

$$M = M_{PEL}\, M'(\lambda,\gamma,\beta,\xi,\alpha,\eta,\mu_{c0},\mu_{c1},\mu_{c2},\mu_{t1},\mu_{t2},\mu_{Ut},\mu_{Uc}) \quad (16)$$

$$\varphi = \varphi_{PEL}\, \varphi'(\lambda,\gamma,\beta,\xi,\alpha,\eta,\mu_{c0},\mu_{c1},\mu_{c2},\mu_{t1},\mu_{t2},\mu_{Ut},\mu_{Uc}) \quad (17)$$

$$\varphi_i'(\lambda,\gamma,\beta,\xi,\alpha,\eta,\mu_{c0},\mu_{c1},\mu_{c2},\mu_{t1},\mu_{t2},\mu_{Ut},\mu_{Uc}) = \frac{\lambda}{2\kappa_i}, \quad i = 1,2,3,\ldots,16 \quad (18)$$

Where M_{PEL} and φ_{PEL} are moment and curvature (for $\gamma = 1$) at the tensile PEL and are defined in Equation (19). Normalized moment for case sixteen (Fig. 2-q) is defined as

$$M_{PEL} = \frac{bh^2 E\varepsilon_{PEL}}{6} \quad , \quad \varphi_{PEL} = \frac{2\varepsilon_{PEL}}{h} \quad (19)$$

$$M_{16}' = -\frac{\kappa_{16}^2}{\lambda^2}(1+\xi\mu_{c2}^3-3\eta\mu_{t2}\lambda^2+\alpha\mu_{t1}^3+3\eta\mu_{t1}\lambda^2+3\beta\mu_{c0}\lambda^2-3\lambda^2+3\mu_{c1}\xi\lambda^2-3\beta\mu_{c1}\lambda^2-\eta\mu_{t1}^3-3\xi\mu_{c2}\lambda^2$$
$$-\xi\mu_{c1}^3+3\alpha\lambda^2-\alpha+\eta\mu_{t2}^3-3\alpha\mu_{t1}\lambda^2-3\gamma\mu_{c0}\lambda^2+\beta\mu_{c1}^3-\beta\mu_{c0}^3+\gamma\mu_{c0}^3)-$$
$$\frac{(-6\alpha\lambda^2+6\lambda^2+6\eta\mu_{t2}\lambda^2+6\alpha\mu_{t1}\lambda^2-6\eta\mu_{t1}\lambda^2)\kappa_{16}}{\lambda^2} - \frac{-3\alpha\mu_{t1}\lambda^2+3\alpha\lambda^2-3\eta\mu_{t2}\lambda^2+3\eta\mu_{t1}\lambda^2-3\lambda^2}{\lambda^2}$$

(20)

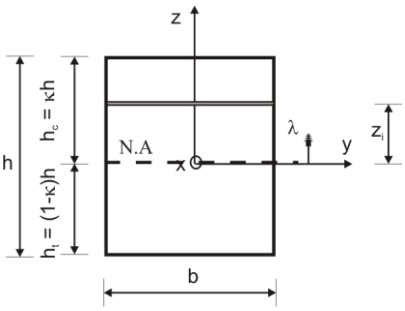

(a) rectangular cross section

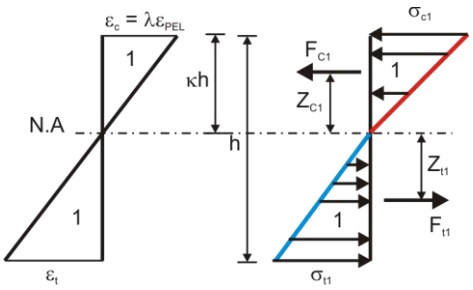

(b) case one

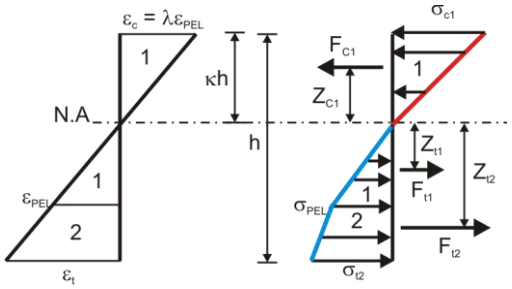

(c) case two

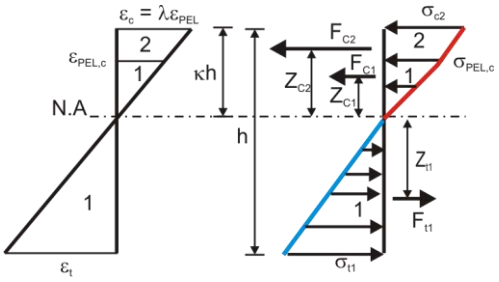

(d) case three

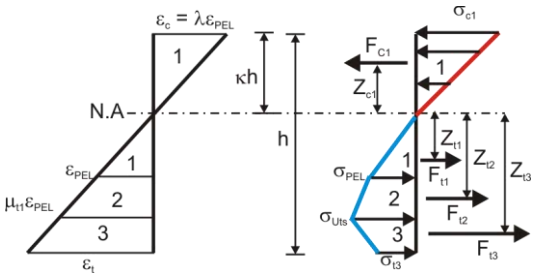

(e) case four

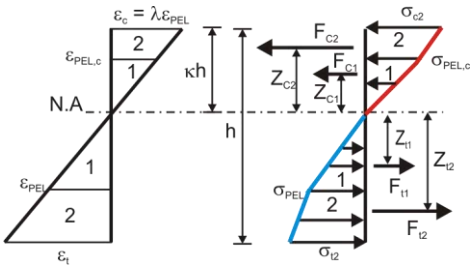

(f) case five

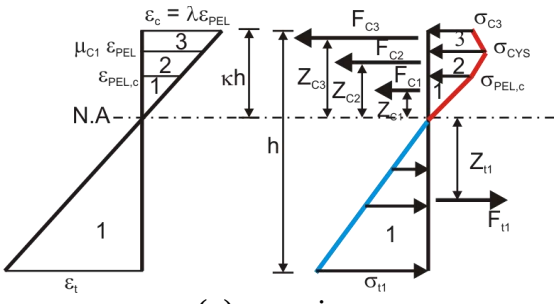

(g) case six

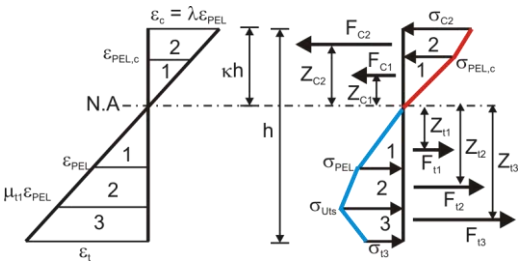

(h) case seven

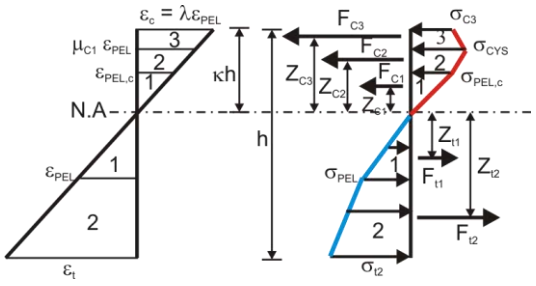

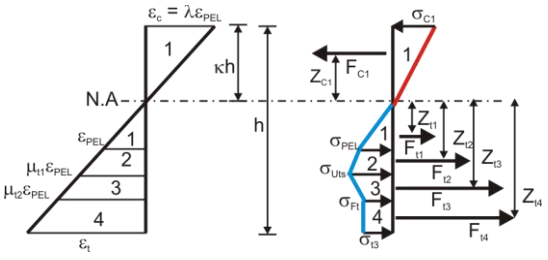

(i) case eight

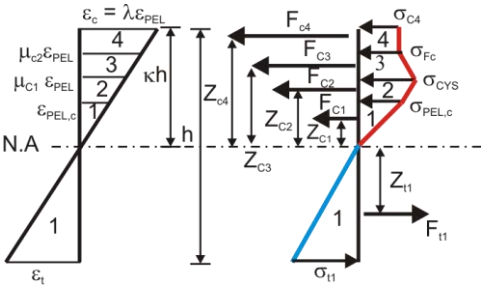

(j) case nine

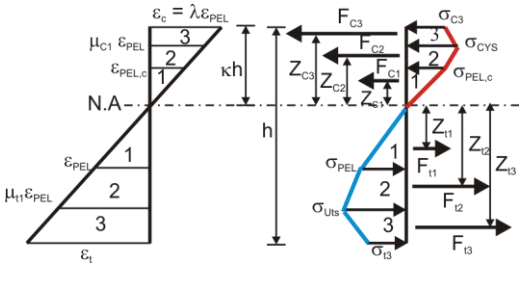

(k) case ten

(l) case eleven

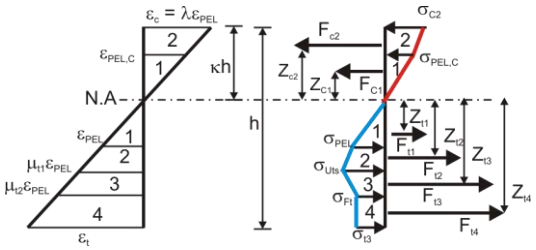

(m) case twelve

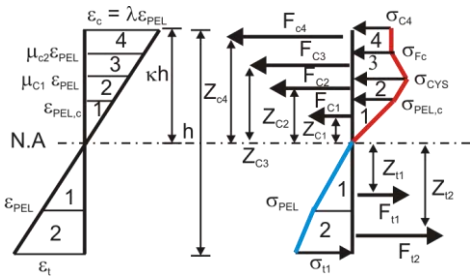

(n) case thirteen

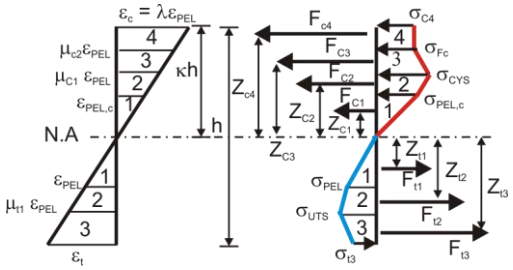

(o) case fourteen

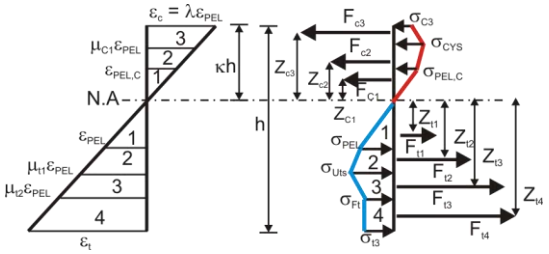

(p) case fifteen

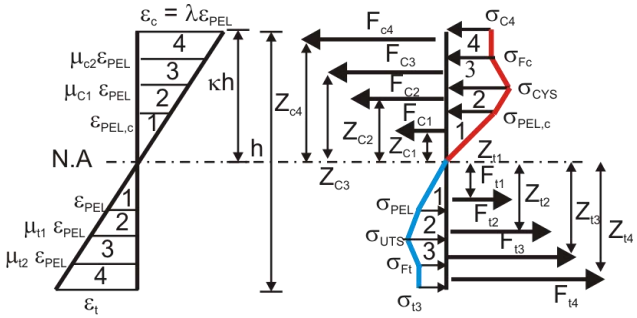

(q) case sixteen

Fig. 2 (a) Rectangular cross section, (b) to (q) sixteen cases of strain and stress distributions.

Table 2: Stress development in the cross section at different stages of flexural loading

Stage	Possible Cases	Transition Point (tp_{ij})
One	One	Min (μ_{c0}, A)
Two	Two	Min (μ_{c0}, C) &
	Three	Min (μ_{c1}, B)
Three	Four	Min (μ_{c0}, F) &
	Five	Min (μ_{c1}, E) &
	Six	Min (μ_{c2}, D)
Four	Seven	Min (μ_{c1}, I) &
	Eight	Min (μ_{c2}, H) &
	Nine	Min (μ_{c0}, J) &
	Ten	Min (μ_{Uc}, G)
Five	Eleven	Min (μ_{c2}, L) &
	Twelve	Min (μ_{c1}, M) &
	Thirteen	Min (μ_{Uc}, K)
Six	Fourteen	Min (μ_{Uc}, N) &
	Fifteen	Min (μ_{c2}, O)
Seven	Sixteen	Min (μ_{Uc}, P)
Eight	failure	

The closed form solutions for the location of neutral axis κ_i, and normalized moment M'_i for all the cases are presented in Tables 3 and 4 in the appendix. The normalized

ultimate moment for a material like resin at very large λ values (M_∞') is computed by substituting $\lambda = \infty$ in the expression for κ in case sixteen in Equation (15) and by substitution of $\lambda = \infty$ and κ_∞ in the normalized moment expression in Equation (20). Equation (21) presents the value of κ for very large λ values. As it is logically expected, the numerator is a function of material parameters in tension while the denominator is a function of both tension and compression parameters. Normalized ultimate moment is obtained as a function of tension and compression material parameters as follows

$$\kappa_\infty = \frac{1+\alpha(\mu_{t1}-1)+\eta(\mu_{t2}-\mu_{t1})}{1+\alpha(\mu_{t1}-1)+\eta(\mu_{t2}-\mu_{t1})+\gamma\mu_{c0}+\beta(\mu_{c1}-\mu_{c0})+\xi(\mu_{c2}-\mu_{c1})} \tag{21}$$

$$M'_\infty = \frac{3(1+\alpha(\mu_{t1}-1)+\eta(\mu_{t2}-\mu_{t1}))(\gamma\mu_{c0}+\beta(\mu_{c1}-\mu_{c0})+\xi(\mu_{c2}-\mu_{c1}))}{(1+\alpha(\mu_{t1}-1)+\eta(\mu_{t2}-\mu_{t1}))+(\gamma\mu_{c0}+\beta(\mu_{c1}-\mu_{c0})+\xi(\mu_{c2}-\mu_{c1}))} \tag{22}$$

Equation (18) clearly shows that normalized curvature would be a very large number for very large λ values. For elastic perfectly plastic materials with equal tensile and compressive elastic moduli and equal yield stress and strain ($\eta = \xi = 0$, $\alpha = \gamma = \beta = 1$, $\mu_{t1} = \mu_{c1} = 1$), Equations (21) and (22) yields to 0.5 and 1.5, respectively, validating the theoretical value that the plastic moment capacity of a rectangular section is 1.5 times of its elastic yield strength (Salmon 1990).

Parametric Study

A set of analytical parametric studies based on developed closed form solutions for moment curvature response is presented. The flexural strength and ductility for each material parameter were expressed as the normalized moment curvature response, which is independent of specimen sizes and PEL strength. Although polymeric materials show strain softening behavior with a percentage of the UTS, a complete set of parametric

studies is conducted to examine the effect of post peak behavior on flexural response. Mechanical characteristic of Epon E 862 epoxy resin was chosen as a base set of parameters (Littell et al., 2008): E = 2069 MPa, Ec = 2457 MPa, ε_{PEL} = 0.0205, ε_{Uts} = 0.076, ε_{St} = 0.16, ε_{Ut} = 0.24, $\varepsilon_{PEL,c}$ = 0.019, ε_{CYS} = 0.092, ε_{Sc} = 0.15, ε_{Uc} = 0.35, σ_{Uts} = 70 MPa, σ_f = 60.5 MPa, σ_{CYS} = 93 MPa, $\sigma_{f,c}$ = 87 MPa

Fig. 3 shows the effect of tensile flow stress on the moment curvature and the location of neutral axis. η = 0.3 and η = 0.001 correspond to tensile plastic flow equal to 25% and almost 100% of the UTS, respectively. Fig. 3 shows that moment curvature response is extremely sensitive to the variations in constant tensile flow as the location of maximum flexure and the post peak regime completely changes with changing tensile plastic flow stress. For the parameters given, Equation (22) yields to η = 0.306 for M' =1; values of η > 0.306 leads to moment capacity at failure less than elastic moment capacity at PEL. In other words, in order to obtain the bending moment at large top compressive strains equal to or greater than the elastic bending capacity, the required tensile plastic flow should be equal to or greater than 25% of the UTS. η = 0.05 exactly characterizes the material behavior of Epon E 862 for which Equation (22) indicates M' = 2.55 at ultimate point. Fig. 3 also shows that decreasing the level of tensile flow decreases the neutral axis depth, especially for η values greater than 0.2. η = 0.2 corresponds to a tensile plastic flow stress equal to 50% of σ_{UTS}. It is observed that the strain softening region of tensile response contributes to the flexural load carrying capacity and nonlinear energy dissipation when subjected to the flexural stress.

Fig. 4 shows the effect of different values of σ_{UTS} at constant ε_{UTS} on the moment curvature and neutral axis location. Since the flow stress in tension is constant, the post

PEL and the softening slopes are calculated for different σ_{UTS} values. The strength gain is almost proportional to σ_{UTS}; the stiffness remains about the same, while ductility slightly increases. However, the amount of M'_{∞} is not affected as much as the flexural strength since for cases α = 0.4, η = 0.16 and α = 0.5, η = 0.226 the moment at infinity is less than the flexural strengths. Fig. 4 illustrates that by increasing the UTS, neutral axis moves downward and exceeds κ = 0.5 for the case of α = 0.5, η = 0.226. Fig. 5 shows the effects of different post PEL slopes, strain at UTS point, and softening slopes with constant σ_{UTS} on flexural response. Results show that changes in the location of the UTS point with a constant value slightly change the moment curvature response. It is observed that the location of the UTS point, for a wide range of normalized top compressive strains between one and four, changes the location of the neutral axis and stress distributions. Fig. 6 illustrates the effect of compressive plastic flow on moment curvature and location of neutral axis. Since the epoxy resin epon E 862 is stronger in compression than tension, changes in compressive plastic flow do not change the moment capacity, but affects the moment at failure considerably. It illustrates that decrease of compression plastic flow increases the neutral axis depth for top compressive strains greater than 0.103. Fig. 7 shows the effects of σ_{CYS} values at constant strain. Like tension, increase of peak strength in compression at constant strain increases the flexural capacity of the epoxy resin. It is observed that change in σ_{CYS} values at constant strain affects moment at failure less than flexural capacity. Results show that an increase of compression peak stress decreases the neutral axis depth considerably.

Researchers have observed different compression behavior in post-peak response for epoxy resins with different specimen shape and dimensions. Strain softening at yield,

followed by strain stiffening at higher strains in compression for different low and high strain rates has been reported (Littell et al. 2008; Jordan et al. 2008; Fiedler et al. 2001; Behzadi and Jones 2005; G'Sell and Souahi 1997; Boyce and Arruda 1990; Buckley and Harding 2001). However, Shah khan et al. (2001) and Chen et al. (2001) didn't observe any strain stiffening at high strains. Fig. 8 illustrates the effect of tension and compression behavior at high strains at stress development at a point of material for epon E 862 under flexural loading. Tensile failure is the governing mechanism for all cases. Materials with $\eta \geq 0.2$ do not experience compression plastic flow and their stress strain relationship in the compression side always is in the ascending region and/or first part of the softening regime. This is the reason that their neutral axis depth and moment capacity drops sharply by increasing the top compressive strain. Results show that shape of stress strain curve for high strain values in compression do not influence the flexural response of materials in which compression is stronger than tension.

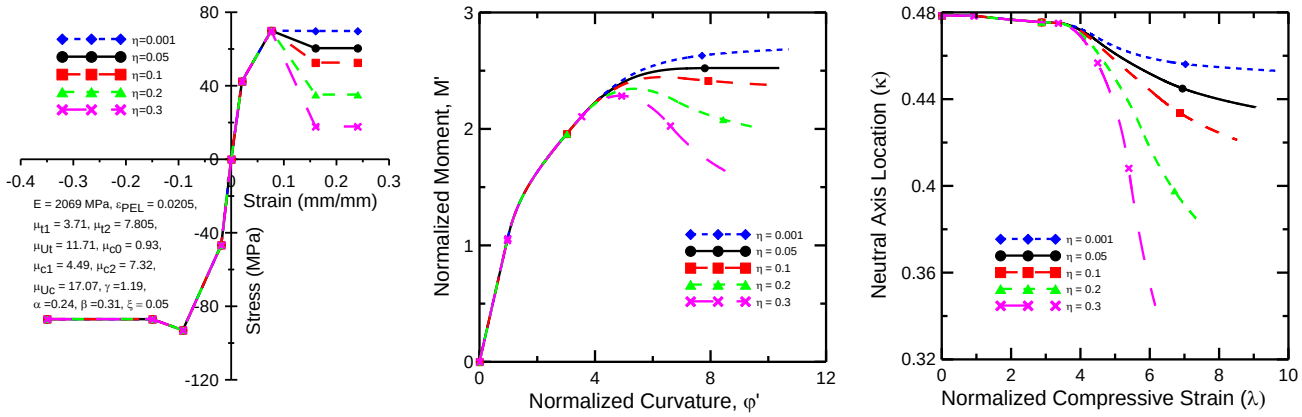

Fig. 3 Effect of tensile flow stress on moment curvature and location of neutral axis

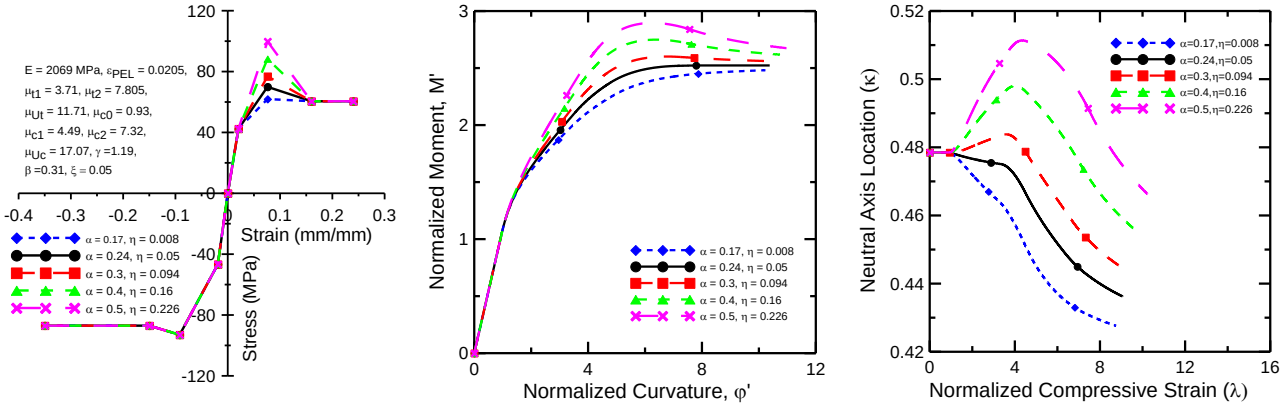

Fig. 4 Effect of σ_{Uts} at constant ε_{Uts} on moment curvature and location of neutral axis

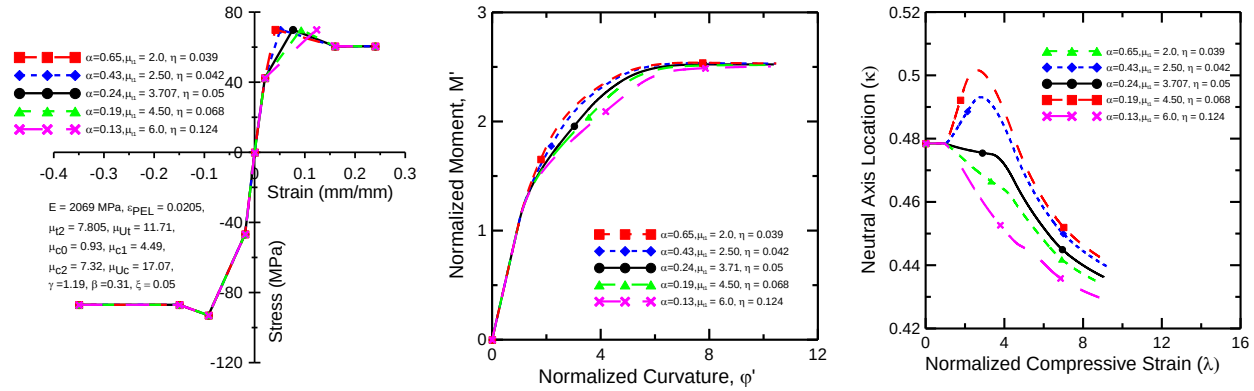

Fig. 5 Effect of post PEL and strain softening slopes at constant σ_{Uts} on flexural response

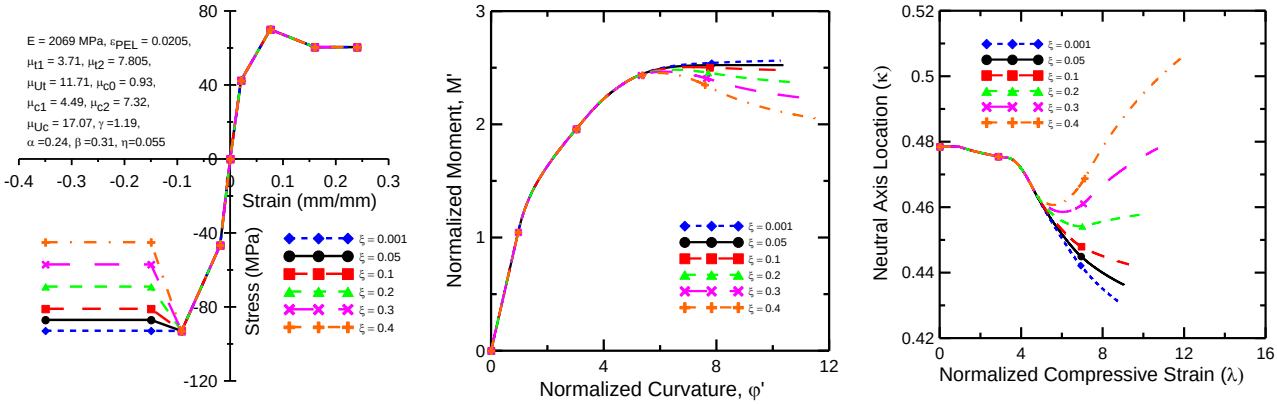

Fig. 6 Effect of compression flow stress on moment curvature and location of neutral axis

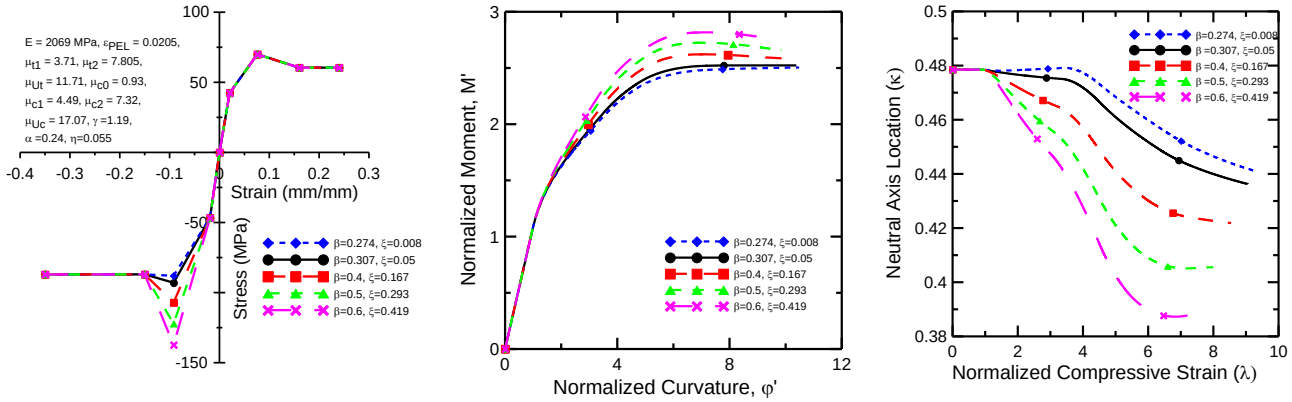

Fig. 7 Effect of σ_{CYS} at constant ε_{CYS} on moment curvature and location of neutral axis

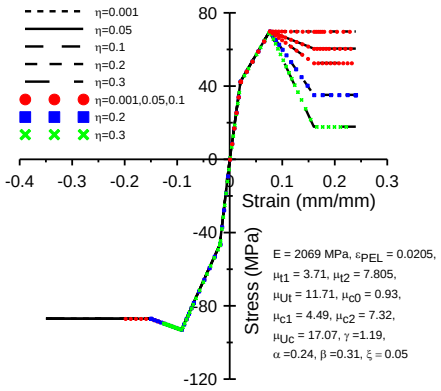

Fig. 8 Effect of tension plastic flow on stress development at a point of material

Load Deflection Algorithm

The load-deflection response is obtained by using the moment curvature response, deformation localization, and the moment area method. In displacement control, the normalized top compressive strain is incrementally imposed to generate a stress distribution profile in a given cross section. For resins, if the compressive strength is greater than the tensile strength, the shape of the moment curvature diagram greatly depends on the value of the post peak tensile stress as observed in the parametric study. Fig. 9 shows a typical moment curvature diagram for epoxy resins which consists of an ascending curve from 0 to M_{max} and a descending curve from M_{max} to $M_{failure}$.

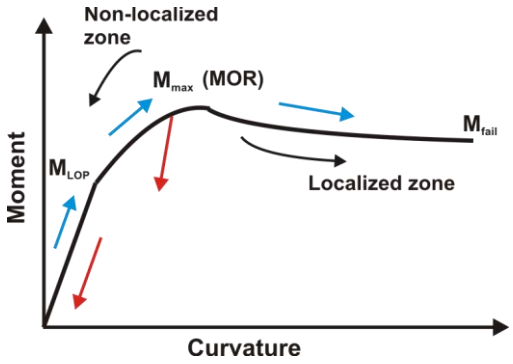

Fig. 9 Moment curvature and crack localization

The first deviation from linearity in a moment curvature or load deflection curve is called Limit of Proportionality (LOP), and the first peak moment or load is called Modulus of Rupture (MOR) as determined in Fig. 9. When a beam is loaded beyond MOR in a material with strain softening behavior, the increase of the deformation decreases load. Polymeric materials are characterized by the existence of a fracture process zone with distributed cracking damage (Bazant and Chen 1997). Fig. 10 shows a 3PB with deformation localization in the cracking region at the vicinity of the load at the groove (region 2) while other zones outside the groove (region 1) undergo unloading during softening. In order to obtain the load deflection response for 3PB from the moment curvature diagram, static equilibrium is used and an array of load steps is derived from a series of discrete data points along a moment curvature diagram. Moment distribution along the length of a beam is obtained by static equilibrium and the corresponding curvature is obtained from a moment curvature relationship. The deflection at the mid span is calculated using moment area method for discrete curvature points at each load step. This procedure is repeated for the number of load steps till a complete load deflection response is obtained.

The specimen is loaded from 0 to P_{LOP} in the ascending portion of the moment curvature diagram from 0 to M_{LOP}. The curvature for this portion is determined directly from the moment curvature diagram. Beyond the LOP, as the specimen undergoes softening, the curvature distribution depends on the localized or non-localized zones and prior strain history. The strain and curvature unloads elastically for an un-cracked section. If the section is loaded beyond M_{LOP}, the unloading curvature of the cracked section follows a quasi-linear recovery path as shown in Fig. 9 and as observed by Littell et al. (2008). Since analytical simulation is done for 3PB under displacement control, cracks do not close when material softens. For sections in the localized zone, the unloading curvature is determined from the descending portion of the moment curvature diagram from M_{max} to $M_{failure}$.

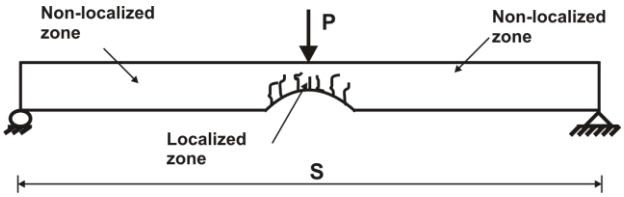

Fig. 10 Crack localization in a beam with groove under a point load at mid span

Simulation of Flexural Load Deflection Response

Tension, compression, and 3PB bending tests were conducted on epoxy resin epon E 863 with a hardener EPI-CURE 3290 using a 100/27 weight ratio at room temperature. Digital image correlation technique, ARAMIS 4M (2006), was used to study the strain fields. Dog bone samples with a 14 mm gage length and an averaged rectangular cross section of 3.18 mm × 3.43 mm were selected to conduct the monotonic tensile tests. Small cubic samples (side 4 mm) were tested under monotonic compression. Small beams with 4mm average width, 10mm thickness, and 60mm length with a groove

(radius of approximately 3.5 mm) in the middle of the beam were selected to conduct 3PB tests. Sections 1 and 2 in Fig. 11 shows that the length of deformation localization at 493 μstr/sec and 59 μstr/sec in the softening stage, obtained from strain field analysis, are 5mm and 4.5 mm, respectively. Figs. 12-a, 12-b, 13-a, and 13-b illustrate the representative experimental tension and compression true stress strain curves at 493 μstr/sec and 59 μstr/sec. Since the compression stress strain curve was not available at 59 μstr/sec, it was built based on the linear relationship between the mechanical characteristics and the logarithm of the strain rate. Experimental results show a strain softening behavior beyond the peak point followed by a constant plateau before failure. A simulation was made to study the load deflection response of epon E 863 and to evaluate the effects of out of plane loading.

The two main parameters and twelve non-dimensional parameters for the models at 493 μstr/sec and 59 μstr/sec are: E = 3049 MPa, ε_{PEL} = 0.0162, μ_{c0} = 1.148, μ_{c1} = 3.52, μ_{c2} = 6.79, μ_{Uc} = 15.70, μ_{t1} = 2.55, μ_{t2} = 8.64, μ_{Ut} = 20.98, γ = 1.09, α = 0.395, β = 0.298, η = -0.0385 and ξ = -0.117 for 493 μstr/sec and E = 2877 MPa, ε_{PEL} = 0.0154, μ_{c0} = 1.331, μ_{c1} = 3.896, μ_{c2} = 6.79, μ_{Uc} = 19.48, μ_{t1} = 2.753, μ_{t2} = 8.05, μ_{Ut} = 19.87, γ = 0.83, α = 0.33, β = 0.285, η = -0.0352 and ξ = -0.122 for 59 μstr/sec. Figs. 12-c and 13-c show the 3PB load deflection curve compared with the simulation results. The figures illustrate that the tension and compression stress strain curves underestimate the load deflection response due to the difference between stress distribution profile in uniaxial tests and bending test. In tension and compression tests, the entire volume of the sample is subjected to the same load and has the same probability of failure. However, in a bending test, only a small fraction of the tension and compression regions are subjected to the

maximum peak stress. Therefore, the probability of crack nucleation, propagation, and failure development in tension and compression samples is higher than in bending samples. Results of the parametric study show that simulation of the flexural response can be improved by changing the ultimate tensile and compressive level and further adjustments of the other parameters. In order to quantify these effects and based on the results of parametric study, one scaling factor (C_1) is proposed to modify the strength of the material.

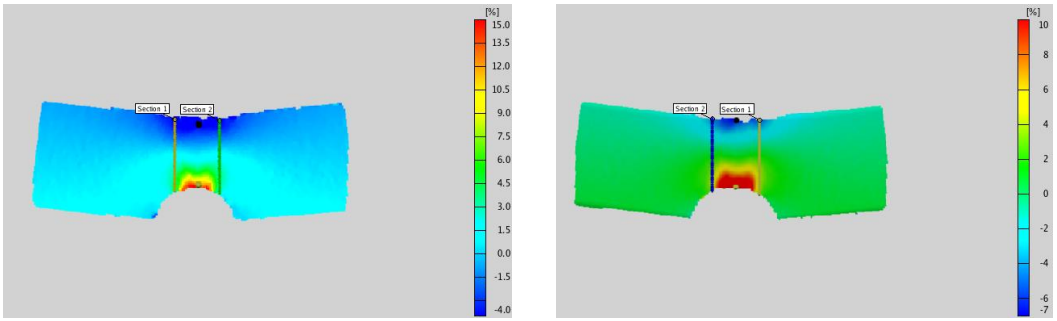

(a) (b)

Fig. 11 Deformation localization area and longitudinal strain distribution (a) 493 μstr/sec; (b) 59 μstr/sec

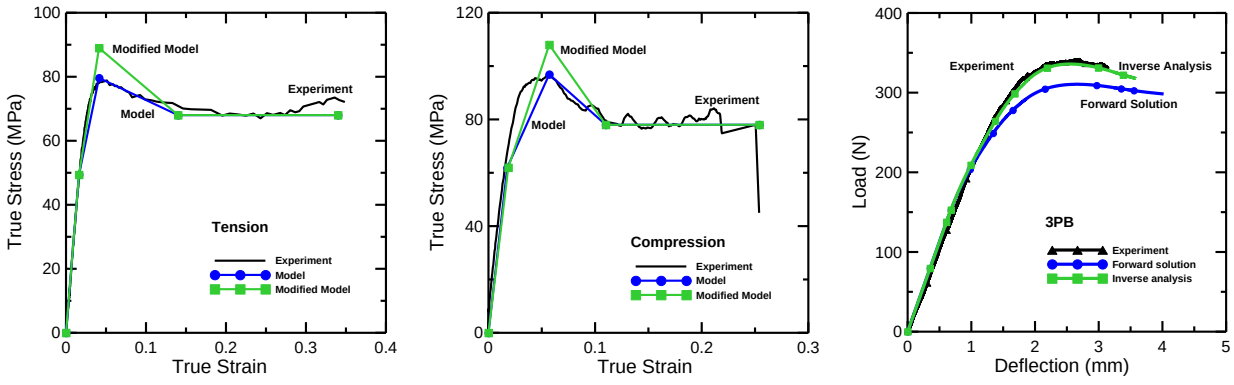

(a) **(b)** **(c)**

Fig. 12 Experiment and simulation of tension, compression and load deflection response at 493 μstr/sec

Various amounts of imperfections in the material directly affect C_1. However, back calculation showed that C_1 for Epon E 863 for 493 μstr/sec and 59 μstr/sec are around 1.14 and 1.24, respectively. An inverse analysis approach of flexural results will establish a statistical relationship between the compression, tension stress strain curves and the flexural response.

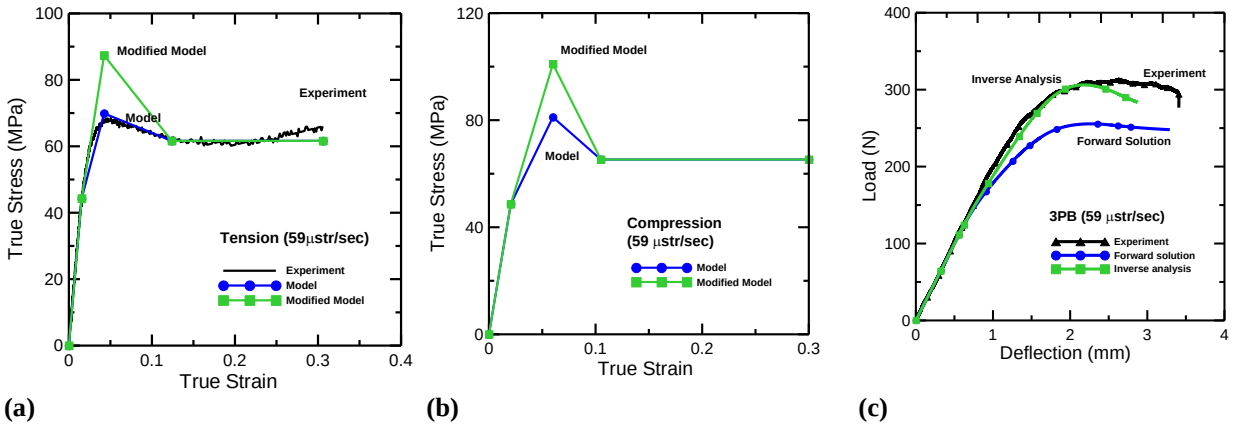

Fig. 13 Experiment and simulation of tension, compression and load deflection response at 59 μstr/sec

Conclusions

Explicit moment curvature equations using nonlinear tension and compression stress strain relation for epoxy resin materials have been developed. A multilinear stress strain relation for epoxy resin materials, consisting of strain softening and flow stress in tension and compression has been used. The material model is described by two intrinsic material parameters: (a) tensile modulus of elasticity, and (b) tensile strain at the PEL point, in addition to five non-dimensional parameters for tension and seven non-dimensional parameters for compression. A parametric study showed that the moment-curvature response is primarily controlled by the post peak tensile and compressive strengths, σ_{UTS}, and σ_{CYS}. It was concluded that compression stress strain parameters have less effect on flexural behavior than tension parameters as long as compression strength is higher than

tension strength. For materials with small post peak tensile strength values, moment at failure is much less than the moment carrying capacity and the response terminate at a relatively low compressive strain. Materials with higher normalized post peak tensile strength have a gradual reduction in the height of the compressive zone, therefore larger deformations are possible. Epoxy resin materials with a considerable amount of post peak tensile strength have a moment capacity around 2.5 times the moment at the PEL point. An increase of σ_{CYS} by increasing the post compressive PEL stiffness at high CYS values, marginally affects the moment capacity in polymeric materials. It is observed that the flexural response in polymeric materials that are stronger in compression than in tension is independent of the shape of the compression stress strain curve at high strain values. Simulation of the load deflection response of epoxy resins in 3PB test revealed the effect of stress gradient on the material behavior. Results indicate that direct use of tension and compression data underestimates the flexural strength. By applying a scaling factor (C_1) to uniaxial tension and compression strength in stress strain curve, flexural behavior of epoxy resins were predicted accurately.

Acknowledgments

The authors gratefully acknowledge the support of this research by the Army Research Office, AMSRD-ARL-RO-SI Proposal Number: 49008-EG, Agreement Number: W911NF-07-1-0132, Program Manager: COL. Reed F. Young.

Notation

b = beam width

E = modulus of elasticity in tension (if $\gamma \neq 1$) or modulus of elasticity (if $\gamma = 1$)

E_c (γ) = modulus of elasticity in compression if $\gamma \neq 1$

$E_{PEL,c}$ (β) = stiffness at the post proportionality limit in compression

$E_{PEL,t}$ (α) = stiffness at the post proportionality limit in tension

$E_{soft,c}$ (ξ) = slope of softening at the post peak region in compression

$E_{soft,t}$ (η) = slope of softening at the post peak region in tension

F_i = force component in each sub-zone (i = 1,2,3,4) of stress diagram

h = beam depth

M_j (M'_j) = moment for each case of stress distribution across the depth

ε_c = compressive strain

ε_{CYS} (μ_{c1}) = strain at the compressive yield strength (peak) point

ε_{PEL} = strain at the proportionality elastic limit point

$\varepsilon_{PEL,c}$ (μ_{c0}) = strain at the proportionality elastic limit point in compression

ε_{Sc} (μ_{c2}) = strain at the end of compressive strain softening point

ε_{St} (μ_{t2}) = strain at the end of tensile strain softening point

ε_t = tensile strain

ε_{Uc} (μ_{Uc}) = strain at the compressive failure point

ε_{Uts} (μ_{t1}) = strain at ultimate tensile strength (peak) point

ε_{Ut} (μ_{Ut}) = strain at the tensile failure point

κ_j = neutral axis depth ratio for each case of stress distribution

λ = normalized applied top compressive strain ($\varepsilon_c / \varepsilon_{PEL}$)

Ω = auxiliary parameter

ϕ_j (ϕ'_j) = curvature for each case of stress distribution across the depth

σ_f = plastic flow stress in tension

$\sigma_{f,c}$ = plastic flow stress in compression

μ_{t1}, μ_{t2}, μ_{Ut}, μ_{co}, μ_{c1}, μ_{c2}, μ_{Uc}, α, η, γ, β, ξ, M'_j, and ϕ'_j are normalized values.

Appendix

Table 3: Neutral axis depth ratio for each case

Case	κ_i
1	$\dfrac{-1+\sqrt{\gamma}}{\gamma-1}$
2	$\dfrac{-\lambda\left(\alpha(\lambda+1)-1-\sqrt{-\alpha+1+\alpha\gamma\lambda^2}\right)}{-\left(\alpha(\lambda+1)^2-2\lambda-1\right)+\gamma\lambda^2}$
3	$\dfrac{\lambda\left(\lambda-\sqrt{(\lambda-\mu_{c0})^2(\beta-\gamma)+\gamma\lambda^2}\right)}{\lambda^2-(\lambda-\mu_{c0})^2(\beta-\gamma)-\gamma\lambda^2}$
4	$\dfrac{\lambda\left(-\eta(\lambda+\mu_{t1})+1+\alpha(\mu_{t1}-1)+\sqrt{1+\alpha^2(\mu_{t1}-1)^2-\eta\alpha(\mu_{t1}-1)^2+2\alpha(\mu_{t1}-1)+\eta\gamma\lambda^2-2\eta\mu_{t1}+\eta}\right)}{\alpha(\mu_{t1}^2-1)+2\lambda+2\alpha\lambda(\mu_{t1}-1)-\eta(\lambda+\mu_{t1})^2+1+\gamma\lambda^2}$
5	$\dfrac{\lambda\left(\alpha(\lambda+1)-1-\sqrt{-\alpha+1+\alpha\left((\lambda-\mu_{c0})^2(\beta-\gamma)+\gamma\lambda^2\right)}\right)}{\alpha(\lambda+1)^2-2\lambda-1-(\lambda-\mu_{c0})^2(\beta-\gamma)-\gamma\lambda^2}$
6	$\dfrac{\lambda\left(-\lambda+\sqrt{\gamma\lambda^2-\gamma(\lambda-\mu_{c0})^2-\beta(\lambda-\mu_{c1})^2+\beta(\lambda-\mu_{c0})^2+\xi(\lambda-\mu_{c1})^2}\right)}{-\lambda^2+\gamma\lambda^2-\gamma(\lambda-\mu_{c0})^2-\beta(\lambda-\mu_{c1})^2+\beta(\lambda-\mu_{c0})^2+\xi(\lambda-\mu_{c1})^2}$
7	$\dfrac{\lambda\left(1+\alpha\mu_{t1}-\alpha-\eta\lambda-\eta\mu_{t1}+\sqrt{1-2\alpha+\eta+2\mu_{t1}(\alpha-\eta)+\eta\gamma\lambda^2+\eta(\lambda-\mu_{c0})(\beta-\gamma)+\alpha(\alpha-\eta)(\mu_{t1}-1)^2}\right)}{(\lambda+\mu_{t1})^2(\alpha-\eta)+(\beta-\gamma)(\lambda-\mu_{c0})^2-\alpha(\lambda+1)^2+\gamma\lambda^2+2\lambda+1}$

8	$$\frac{\lambda\left(\alpha(\lambda+1)-1-\sqrt{\alpha(\beta-\gamma)(\lambda-\mu_{c0})^2+\alpha(\xi-\beta)(\lambda-\mu_{c1})^2+\alpha\gamma\lambda^2-\alpha+1}\right)}{(\lambda-\mu_{c0})^2(\gamma-\beta)+(\beta-\xi)(\lambda-\mu_{c1})^2-\gamma\lambda^2+\alpha(\lambda+1)^2-2\lambda-1}$$
9	$$\frac{2\lambda(1+\alpha(\mu_{t1}-1)+\eta(\mu_{t2}-\mu_{t1}))}{1+2\lambda+\gamma\lambda^2+(\lambda+\mu_{t1})^2(\alpha-\eta)+\eta(\lambda+\mu_{t2})^2-\alpha(\lambda+1)^2}$$
10	$$\frac{\lambda\left(\lambda-\sqrt{(\lambda-\mu_{c1})^2(-\beta+\xi)+(-\gamma+\beta)(\lambda-\mu_{c0})^2+\gamma\lambda^2-\xi(\lambda-\mu_{c2})^2}\right)}{(\lambda-\mu_{c1})^2(\beta-\xi)+(\gamma-\beta)(\lambda-\mu_{c0})^2+\lambda^2(1-\gamma)+\xi(\lambda-\mu_{c2})^2}$$
11	$$\frac{\lambda(-\eta\lambda-\eta\mu_{t1}+1+\alpha\mu_{t1}-\alpha)}{-\alpha(\lambda+1)^2+(\alpha-\eta)(\lambda+\mu_{t1})^2+(\xi-\beta)(\lambda-\mu_{c1})^2+(\beta-\gamma)(\lambda-\mu_{c0})^2+\gamma\lambda^2+2\lambda+1}$$ $$+\frac{\lambda\sqrt{\eta(\lambda-\mu_{c0})^2(\beta-\gamma)+\eta(\lambda-\mu_{c1})^2(\xi-\beta)+\alpha(\mu_{t1}-1)^2(\alpha-\eta)+\eta\gamma\lambda^2+2\alpha\mu_{t1}-2\eta\mu_{t1}+\eta-2\alpha+1}}{-\alpha(\lambda+1)^2+(\alpha-\eta)(\lambda+\mu_{t1})^2+(\xi-\beta)(\lambda-\mu_{c1})^2+(\beta-\gamma)(\lambda-\mu_{c0})^2+\gamma\lambda^2+2\lambda+1}$$
12	$$\frac{2\lambda(1+\alpha(\mu_{t1}-1)+\eta(\mu_{t2}-\mu_{t1}))}{\alpha(\lambda+\mu_{t1})^2-\alpha(\lambda+1)^2+(\beta-\gamma)(\lambda-\mu_{c0})^2+2\eta\lambda(\mu_{t2}-\mu_{t1})+\eta(\mu_{t2}^2-\mu_{t1}^2)+\gamma\lambda^2+2\lambda+1}$$
13	$$\frac{\lambda\left(\alpha\lambda+\alpha-1-\sqrt{\alpha(\lambda-\mu_{c0})^2(\beta-\gamma)+\alpha(\lambda-\mu_{c1})^2(\xi-\beta)-\alpha\xi(\lambda-\mu_{c2})^2+\alpha\gamma\lambda^2-\alpha+1}\right)}{(\lambda-\mu_{c0})^2(\gamma-\beta)+(\lambda-\mu_{c1})^2(\beta-\xi)+\xi(\lambda-\mu_{c2})^2+\alpha(\lambda+1)^2-\gamma\lambda^2-2\lambda-1}$$
14	$$\frac{-\lambda(\eta\lambda+\eta\mu_{t1}+\alpha-\alpha\mu_{t1}-1)}{(\lambda-\mu_{c0})^2(\beta-\gamma)+(\lambda-\mu_{c1})^2(\xi-\beta)-\xi(\lambda-\mu_{c2})^2+(\lambda+\mu_{t2})^2(\alpha-\eta)-\alpha(\lambda+1)^2+\gamma\lambda^2+2\lambda+1}$$ $$+\frac{\lambda\sqrt{\eta(\lambda-\mu_{c0})^2(\beta-\gamma)+\eta(\lambda-\mu_{c1})^2(\xi-\beta)-\eta\xi(\lambda-\mu_{c2})^2+\alpha(\mu_{t1}-1)^2(\alpha-\eta)+2\alpha(\mu_{t1}-1)+\eta\gamma\lambda^2-2\eta\mu_{t1}+\eta+1}}{(\lambda-\mu_{c0})^2(\beta-\gamma)+(\lambda-\mu_{c1})^2(\xi-\beta)-\xi(\lambda-\mu_{c2})^2+(\lambda+\mu_{t2})^2(\alpha-\eta)-\alpha(\lambda+1)^2+\gamma\lambda^2+2\lambda+1}$$
15	$$\frac{2\lambda(1+\alpha(\mu_{t1}-1)+\eta(\mu_{t2}-\mu_{t1}))}{(\lambda-\mu_{c0})^2(\beta-\gamma)+(\xi-\beta)(\lambda-\mu_{c1})^2+(\lambda+\mu_{t1})^2(\alpha-\eta)+\eta(\lambda+\mu_{t2})^2-\alpha(\lambda+1)^2+\gamma\lambda^2+2\lambda+1}$$
16	$$\frac{-2\lambda(1+\alpha(\mu_{t1}-1)+\eta(\mu_{t2}-\mu_{t1}))}{(\lambda-\mu_{c0})^2(\gamma-\beta)+(\lambda-\mu_{c1})^2(\beta-\xi)+\xi(\lambda-\mu_{c2})^2+(\lambda+\mu_{t1})^2(\eta-\alpha)-\eta(\lambda+\mu_{t2})^2+\alpha(\lambda+1)^2-\gamma\lambda^2-2\lambda-1}$$

Table 4: Normalized moment for each case

Case	M'_i
1	$2\lambda(\gamma-1)\kappa_1^{\,2}+6\lambda\kappa_1-6\lambda+\frac{2\lambda}{\kappa_1}$
2	$\frac{\left((1-\alpha)\left(3\lambda^2-1\right)-2\lambda^3(\alpha-\gamma)\right)\kappa_2^2}{\lambda^2}+6\left(\alpha(\lambda+1)-1\right)\kappa_2+3\left(1-\alpha(1+2\lambda)\right)+\frac{2\alpha\lambda}{\kappa_2}$
3	$\frac{(-\gamma\mu_{c0}^3-3\mu_{c0}\beta\lambda^2+3\gamma\mu_{c0}\lambda^2+2\beta\lambda^3+\beta\mu_{c0}^3-2\lambda^3)\kappa_3^{\,2}}{\lambda^2}+6\lambda\kappa_3-6\lambda+\frac{2\lambda}{\kappa_3}$
4	$\frac{(3\lambda^2\alpha\mu_{t1}+\mu_{t1}^3\eta-1-3\mu_{t1}\eta\lambda^2+2\gamma\lambda^3+\alpha-3\alpha\lambda^2-2\eta\lambda^3+3\lambda^2-\alpha\mu_{t1}^3)\kappa_4^{\,2}}{\lambda^2}+$ $(6\alpha+6\eta\lambda+6\mu_{t1}\eta-6-6\alpha\mu_{t1})\kappa_4+-3\mu_{t1}\eta+3-6\eta\lambda+3\alpha\mu_{t1}-3\alpha+\frac{2\eta\lambda}{\kappa_4}$
5	$\frac{(-\gamma\mu_{c0}^3-3\mu_{c0}\beta\lambda^2+3\gamma\mu_{c0}\lambda^2+2\beta\lambda^3+\beta\mu_{c0}^3-1-2\alpha\lambda^3+\alpha+3\lambda^2-3\alpha\lambda^2)\kappa_5^{\,2}}{\lambda^2}$ $+(-6+6\alpha\lambda+6\alpha)\kappa_5-3\alpha-6\alpha\lambda+3+\frac{2\alpha\lambda}{\kappa_5}$
6	$\frac{(-\gamma\mu_{c0}^3+3\gamma\mu_{c0}\lambda^2-\beta\mu_{c1}^3+\beta\mu_{c0}^3-3\mu_{c1}\xi\lambda^2+\xi\mu_{c1}^3+3\beta\mu_{c1}\lambda^2-3\beta\mu_{c0}\lambda^2+2\xi\lambda^3-2\lambda^3)\kappa_6^{\,2}}{\lambda^2}$ $+6\lambda\kappa_6-6\lambda+\frac{2\lambda}{\kappa_6}$
7	$\frac{(\alpha+3\lambda^2+3\lambda^2\alpha\mu_{t1}+2\beta\lambda^3-\gamma\mu_{c0}^3+\beta\mu_{c0}^3-3\mu_{c0}\beta\lambda^2-\alpha\mu_{t1}^3+\mu_{t1}^3\eta-3\alpha\lambda^2-2\lambda^3\eta-1+3\gamma\mu_{c0}\lambda^2-3\mu_{t1}\eta\lambda^2)\kappa_7^{\,2}}{\lambda^2}$ $+(6\lambda\eta+6\mu_{t1}\eta-6-6\alpha\mu_{t1}+6\alpha)\kappa_7+3\alpha\mu_{t1}-6\lambda\eta+3-3\mu_{t1}\eta-3\alpha+\frac{2\eta\lambda}{\kappa_7}$
8	$-\frac{(1-3\gamma\mu_{c0}\lambda^2-3\beta\mu_{c1}\lambda^2+3\mu_{c1}\xi\lambda^2+\beta\mu_{c1}^3-\beta\mu_{c0}^3+3\beta\mu_{c0}\lambda^2+\gamma\mu_{c0}^3-\xi\mu_{c1}^3+3\alpha\lambda^2-\alpha-2\xi\lambda^3+2\alpha\lambda^3-3\lambda^2)\kappa_8^{\,2}}{\lambda^2}$ $-(6-6\alpha\lambda-6\alpha)\kappa_8-\left(3\alpha-3+6\alpha\lambda\right)+\frac{2\alpha\lambda}{\kappa_8}$

9	$\frac{(3\lambda^2\alpha\mu_{t1}+3\eta\mu_{t2}\lambda^2-3\mu_{t1}\eta\lambda^2+\alpha-\alpha\mu_{t1}^3+\mu_{t1}^3\eta-\eta\mu_{t2}^3-3\alpha\lambda^2-1+2\gamma\lambda^3+3\lambda^2)\kappa_9{}^2}{\lambda^2}$ $+(-6\eta\mu_{t2}-6-6\alpha\mu_{t1}+6\alpha+6\mu_{t1}\eta)\kappa_9+3\alpha\mu_{t1}-3\mu_{t1}\eta+3+3\eta\mu_{t2}-3\alpha$
10	$-\frac{(\beta\mu_{c1}^3-\xi\mu_{c1}^3-\beta\mu_{c0}^3+\gamma\mu_{c0}^3+\xi\mu_{c2}^3+2\lambda^3-3\gamma\mu_{c0}\lambda^2-3\beta\mu_{c1}\lambda^2+3\beta\mu_{c0}\lambda^2-3\xi\mu_{c2}\lambda^2+3\xi\mu_{c1}\lambda^2)\kappa_{10}{}^2}{\lambda^2}+6\lambda\kappa_{10}$ $-6\lambda+\frac{2\lambda}{\kappa_{10}}$
11	$-\frac{1}{\lambda^2}(-\alpha+1-3\lambda^2-2\xi\lambda^3+2\eta\lambda^3-3\gamma\mu_{c0}\lambda^2-\beta\mu_{c0}^3+3\xi\mu_{c1}\lambda^2-\mu_{t1}^3\eta+3\mu_{t1}\eta\lambda^2+3\beta\mu_{c0}\lambda^2+3\alpha\lambda^2-3\alpha\mu_{t1}\lambda^2$ $-3\beta\mu_{c1}\lambda^2+\beta\mu_{c1}^3+\gamma\mu_{c0}^3-\xi\mu_{c1}^3+\alpha\mu_{t1}^3)\kappa_{11}{}^2-(-6\eta\lambda+6+6\alpha\mu_{t1}-6\mu_{t1}\eta-6\alpha)\kappa_{11}$ $+3\alpha\mu_{t1}-6\eta\lambda-3\alpha+3-3\mu_{t1}\eta+\frac{2\eta\lambda}{\kappa_{11}}$
12	$\frac{1}{\lambda^2}(3\gamma\mu_{c0}\lambda^2-3\mu_{t1}\eta\lambda^2+2\beta\lambda^3+\alpha-\alpha\mu_{t1}^3-\gamma\mu_{c0}^3-\eta\mu_{t2}^3+\beta\mu_{c0}^3-3\beta\mu_{c0}\lambda^2+\mu_{t1}^3\eta+3\lambda^2-1+3\alpha\mu_{t1}\lambda^2$ $-3\alpha\lambda^2+3\eta\mu_{t2}\lambda^2)\kappa_{12}{}^2+(6\alpha+6\mu_{t1}\eta-6-6\alpha\mu_{t1}-6\eta\mu_{t2})\kappa_{12}-3\mu_{t1}\eta+3\alpha\mu_{t1}-3\alpha+3+3\eta\mu_{t2}$
13	$\frac{1}{\lambda^2}(\beta\mu_{c0}^3+\xi\mu_{c1}^3-\beta\mu_{c1}^3+\alpha+3\lambda^2-3\alpha\lambda^2-\gamma\mu_{c0}^3-1-\xi\mu_{c2}^3+3\gamma\mu_{c0}\lambda^2+3\beta\mu_{c1}\lambda^2-3\beta\mu_{c0}\lambda^2+3\xi\mu_{c2}\lambda^2$ $-3\xi\mu_{c1}\lambda^2-2\alpha\lambda^3)\kappa_{13}{}^2+(-6+6\alpha\lambda+6\alpha)\kappa_{13}+3-3\alpha-6\alpha\lambda+\frac{2\alpha\lambda}{\kappa_{13}}$
14	$\frac{1}{\lambda^2}(3\xi\mu_{c2}\lambda^2-3\xi\mu_{c1}\lambda^2-3\mu_{t1}\eta\lambda^2-\gamma\mu_{c0}^3+3\beta\mu_{c1}\lambda^2+\alpha+\beta\mu_{c0}^3+3\gamma\mu_{c0}\lambda^2+3\alpha\mu_{t1}\lambda^2-3\beta\mu_{c0}\lambda^2-3\alpha\lambda^2$ $+\mu_{t1}^3\eta+3\lambda^2-2\eta\lambda^3-\xi\mu_{c2}^3+\xi\mu_{c1}^3-\alpha\mu_{t1}^3-1-\beta\mu_{c1}^3)\kappa_{14}{}^2+(-6+6\alpha-6\alpha\mu_{t1}+6\mu_{t1}\eta+6\eta\lambda)\kappa_{14}$ $-3\mu_{t1}\eta+3+3\alpha\mu_{t1}-6\eta\lambda-3\alpha+\frac{2\eta\lambda}{\kappa_{14}}$
15	$-\frac{1}{\lambda^2}(1+\beta\mu_{c1}^3-\beta\mu_{c0}^3-3\alpha\mu_{t1}\lambda^2+\gamma\mu_{c0}^3+3\alpha\lambda^2-2\xi\lambda^3+\alpha\mu_{t1}^3-\eta\mu_{t1}^3+\eta\mu_{t2}^3+3\mu_{c1}\xi\lambda^2-3\gamma\mu_{c0}\lambda^2-3\beta\mu_{c1}\lambda^2$ $+3\beta\mu_{c0}\lambda^2-3\eta\mu_{t2}\lambda^2-\alpha+3\eta\mu_{t1}\lambda^2-3\lambda^2-\xi\mu_{c1}^3)\kappa_{15}{}^2-(-6\alpha+6+6\eta\mu_{t2}+6\alpha\mu_{t1}-6\eta\mu_{t1})\kappa_{15}$ $+3\alpha\mu_{t1}-3\alpha+3\eta\mu_{t2}-3\eta\mu_{t1}+3$

16	$-\frac{1}{\lambda^2}(1+\xi\mu_{c2}^3-3\eta\mu_{t2}\lambda^2+\alpha\mu_{t1}^3+3\eta\mu_{t1}\lambda^2+3\beta\mu_{c0}\lambda^2-3\lambda^2+3\mu_{c1}\xi\lambda^2-3\beta\mu_{c1}\lambda^2-\eta\mu_{t1}^3-3\xi\mu_{c2}\lambda^2-\xi\mu_{c1}^3$ $+3\alpha\lambda^2-\alpha+\eta\mu_{t2}^3-3\alpha\mu_{t1}\lambda^2-3\gamma\mu_{c0}\lambda^2+\beta\mu_{c1}^3-\beta\mu_{c0}^3+\gamma\mu_{c0}^3)\kappa_{16}{}^2-(-6\alpha+6+6\eta\mu_{t2}+6\alpha\mu_{t1}-6\eta\mu_{t1})\kappa_{16}$ $+3\alpha\mu_{t1}-3\alpha+3\eta\mu_{t2}-3\eta\mu_{t1}+3$

References

Ward, I. M., and Sweeney, J. (2004). "Mechanical properties of solid polymers." *John Wiley & Sons.*

Buckley, C.P., and Jones, D.C., (1995). "Glass-rubber constitutive model for amorphous polymers near the glass transition" *Polymer,* 36, 3301-3312.

Buckley, C.P., Dooling, P.J., (2004). "Deformation of thermosetting resins at impact rates of strain, part 2." *J Mech Phys Solids,* 52(10), 2355–2377.

Boyce, M.C., Parks, D.M., and Argon, A.S., (1989). "Plastic flow in oriented glassy polymers." *Int J Plasticity,* 5, 593, 615.

Boyce, M.C., Arruda, E.M., and Jayachandran, R., (1994). "The large strain compression, tension, and simple shear of polycarbonate" *Polym Eng Sci*, 34, 716-725.

Hasan, O.A., Boyce, M.C., (1995). "A constitutive model for the nonlinear viscoelastic viscoplastic behavior of glassy polymers" *Polym Eng Sci*, 35, 331-344.

Mulliken, A.D., and Boyce, M.C., (2006). "Mechanics of the rate-dependent elastic-plastic deformation of glassy polymers from low to high strain rates" *Int J Solids Struct*, 43, 1331–1356.

Tervoort, T.A., Klompen, E.T.J., and Govaert, L.E., (1996). "A multi-mode approach to finite 3D nonlinear viscoelastic behavior of polymers" *J. Rheol*. 40, 779-797.

Tervoort, T.A., Smit, R.J.M., Brekelmans, W.A.M., and Govaert, L.E., (1998). "A constitutive equation for the elasto-viscoplastic deformation of glassy polymers" *Mech Time-Depend Mater*, 1, 269-291.

Govaert, L.E., Timmermans, P.H.M., and Brekelmans, W.A.M., (2000). "The influence of intrinsic strain softening on strain localization in polycarbonate: modeling and experimental validation" *J Eng Mater-T ASME*, 122, 177-185.

Wineman, A.S., and Rajagopal, K. R. (2000). "Mechanical Response of Polymers" *Cambridge Univeristy Press, New York*.

Zhang, C., and Moore, I.D., (1997). "Nonlinear mechanical response of high density polyethylene. Part II: uniaxial constitutive modeling" *Polym Eng Sci*, 37, 414-420.

Gilat, A., Goldberg, R.K., and Roberts, G.D., (2007). "Strain rate sensitivity of epoxy resin in tensile and shear loading" *J. Aerospace Eng.*, 75-89.

Li, F.Z., and Pan, J., (1990). "Plane stress crack-tip fields for pressure sensitive dilatant materials," *J. Appl. Mech.*, 57, 40-49.

Chang, W.J., and Pan, J., (1997). "Effects of yield surface shape and round-off vertex on crack-tip fields for pressure sensitive materials," *Int. J. Solids Struct.*, 34, 3291-3320.

Hsu, S.Y., Vogler, T.J., and Kyriakides, S., (1999) "Inelastic behavior of an AS4/PEEK composite under combined transverse compression and shear" *Int. J. Plast*., 15, 807-836.

Jordan, J.L., Foley, J.R., and Siviour, C.R. (2008). "Mechanical properties of epon 826/DEA epoxy" *Mech Time-Depend Mater.*, 12, 249-272.

Lu, H., Tan, G., and Chen, W., (2001). "Modeling of constitutive behavior for Epon 828/T-403 at high strain rates" *Mech Time-Depend Mater.*, 5, 119-130.

Chen, W., and Zhou, B., (1998). "Constitutive behavior of Epon 828/T-403 at various strain rates" *Mech Time-Depend Mater*, 2, 103-111.

Johnson, G.R., Hoegfeldt, J.M., Lindholm, U.S., and Nagy, A., (1983). "Response of various metals to large torsional strains over a large range of strain rates- Part 1: ductile metals" *Transactions of the ASME, J Eng Mater-T ASME*, 105, 42-47.

Naaman, A. E., and Reinhardt, H.W., (2006). "Proposed classification of HPFRC composites based on their tensile response." *Mater Struct*, 39, 547-555

Hobbiebrunken, T., Fiedler, B., Hojo, M., and Tanaka, M., (2007). "Experimental determination of the true epoxy resin strength using micro-scaled specimens" *Compos Part A*, 38, 814-818.

Goodier, JN., (1933). "Concentration of stress around spherical and cylindrical inclusions and flaws" *Trans Am Soc Mech Eng*, 55, 39-44.

Bazant, Z.P., and Chen, E., (1997). "Scaling of structural failure" *Appl Mech.*, 593-627

Odom, E.M., and Adams, D.F., (1992). "Specimen size effect during tensile testing of an unreinforced polymer" *J Mater Sci*., 27, 1767-1771.

Giannotti, M.I., Galante, M.J., Oyanguren, P.A., and Vallo, C.I., (2003). "Role of intrinsic flaws upon flexural behavior of a thermoplastic modified epoxy resin." *Polym Test*, 22, 429-437.

Vallo, C.I., (2002). "Influence of load type on flexural strength of a bone cement based on PMMA" *Polym Test*, 21, 793-800.

G'Sell, C., Souahi, A. (1997). "Influence of cross linking on the plastic behavior of amorphous polymers at large strains." *J Eng Mater-T*, 119, 223-227.

Boyce, M.C., Arruda, E.M. (1990). “An experimental and analytical investigation of the large strain compressive and tensile response of glassy polymers.” *Polym Eng Sci*, 30, 1288-1298

Buckley, C.P., Harding, J. (2001). “Deformation of thermosetting resins at impact rates of strain, Part I: experimental study.” *J Mech Phys Solids*, 49(7), 1517–1538.

Shah Khan, M.Z., Simpson, G., and Townsend, C.R. (2001). “A comparison of the mechanical properties in compression of two resins.” *Mater Lett*, 52, 173-179.

Littell, J.D., Ruggeri, C.R., Goldberg, R.K., Roberts, G.D., Arnold, W.A., and Binienda, W.K. (2008). “Measurement of epoxy resin tension, compression, and shear stress- strain curves over a wide range of strain rates using small test specimens” *J. Aerospace Eng.*, 162-173.

Chen, W., Lu, F., and Cheng, M. (2001). “Tension and compression tests of two polymers under quasi-static and dynamic loading.” *Polym Test*, 21, 113-121.

Foreman, J.P., Porter, D., Behzadi, S., Curtis, P.T., and Jones, F.R., (2010) “Predicting the thermomechanical properties of an epoxy resin blend as a function of temperature and strain rate” *Compos Part A*, 41, 1072-1076

Salmon, C.G., and Johnson, J.E., (1990). “Steel Structures: Design and behavior.” *3rd edition, Harper and Row, New York*

Fiedler, B., Hojo, M., Ochiai, S., and Ando, M. (2001). “Failure behavior of an epoxy matrix under different kinds of static loading.” *Compos Sci Technol*, 61, 1615-1624.

Behzadi, S., and Jones, F. (2005). “Yielding behavior of model epoxy matrices for fiber reinforced composites: Effect of strain rate and temperature.” *J Macromol Sci Phys*. 993-1005.

ARAMIS (2006). “User’s manual for3-D image photogrammetry”.